

On the thermal sunset diagram for scalar field theories

Tetsuo NISHIKAWA,^{*} Osamu MORIMATSU,[†] and Yoshimasa HIDAKA[‡]

*Institute of Particle and Nuclear Studies,
High Energy Accelerator Research Organization,
1-1, Oho, Tsukuba, Ibaraki, 305-0801, Japan*

(Dated: September 3, 2018)

arXiv:hep-ph/0302098v1 13 Feb 2003

Abstract

We study the so-called “sunset diagram”, which is one of two-loop self-energy diagrams, for scalar field theories at finite temperature.

For this purpose, we first find the complete expression of the bubble diagram, the one-loop subdiagram of the sunset diagram, for arbitrary momentum. The temperature-dependent discontinuous part as well as the well-known temperature independent part is obtained analytically. The continuous part is reduced to a one-dimensional integral which one can easily evaluate numerically.

We calculate the temperature independent part and dependent part of the sunset diagram separately. For the former, we obtain the discontinuous part first and the finite continuous part next using a twice-subtracted dispersion relation. For the latter, we express it as a one-dimensional integral in terms of the bubble diagram.

We also study the structure of the discontinuous part of the sunset diagram. Physical processes, which are responsible for it, are identified. Processes due to the scattering with particles in the heat bath exist only at finite temperature and generate discontinuity for arbitrary momentum, which is a remarkable feature of the two-loop diagrams at finite temperature.

As an application of our result, we study the effect of the diagram on the spectral function of the sigma meson at finite temperature in the linear sigma model, which was obtained at one-loop order previously. At high temperature where the decay $\sigma \rightarrow \pi\pi$ is forbidden, sigma acquires a finite width of the order of 10 MeV while within the one-loop calculation its width vanishes. At low temperature, the spectrum does not deviate much from that at one-loop order. Possible consequences with including other two-loop diagrams are discussed.

PACS numbers: 11.10.Wx, 12.40.-y, 14.40.Aq, 14.40.Cs, 25.75.-q

Keywords: sigma meson, two-loop self-energy, spectral function, finite temperature, linear sigma model

*Electronic address: nishi@post.kek.jp

†Electronic address: osamu.morimatsu@kek.jp

‡Electronic address: hidaka@post.kek.jp

I. INTRODUCTION

The so-called sunset diagram, which is depicted in Fig.1, is one of two-loop self-energy diagrams. The sunset diagram appears in theories with 4-point vertices such as $\mathcal{O}(4)$ linear sigma model, ϕ^4 theory, and so on.

At finite temperature, two-loop self-energy diagrams have remarkable features that are not seen at zero temperature. Consider the discontinuity of the self-energy. At zero temperature, the discontinuity of one-loop diagrams is due to two particle intermediate states and that of two-loop diagrams comes from three particle states in addition to two particle ones. In general, in higher loop diagrams new processes appear. However, they contribute to the discontinuity only at higher energies. On the other hand, at finite temperature, even though the number of particles participating in the process at a given order of loops is the same as that at zero temperature, new processes appear even at low energy. This is because at finite temperature some of particles participating in the process can be particles in the heat bath. Furthermore, as will be shown in this paper, there exist processes which are possible at arbitrary energy. Accordingly, the discontinuity of two-loop self-energies is non-vanishing in all the energy region. Therefore, in some cases at finite temperature, to extend calculations to two-loop order has a meaning more than just making more precision.

One of such cases is the spectral function for the sigma meson in the linear sigma model. The spectral function of the sigma meson at finite temperature was studied by Chiku and Hatsuda at one-loop level [1]. The sigma meson at zero temperature has a large width due to the strong coupling with two pions. However, they found that at finite temperature the spectral function near $\sigma \rightarrow \pi\pi$ threshold is enhanced as a typical signal of chiral phase transition. This is because, as the temperature increases, the mass of σ decreases while that

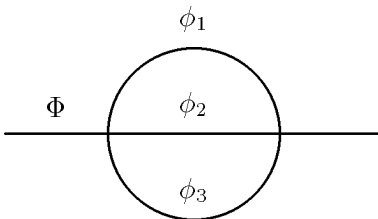


FIG. 1: “Sunset” diagram. We label the external particle by “ Φ ” and internal particles with mass m_i by ϕ_i .

of π increases due to partial restoration of chiral symmetry and, accordingly, the phase space available for the $\sigma \rightarrow \pi\pi$ decay is squeezed to zero. At finite temperature, however, there exist processes, collision with or absorption of a thermal particle in the heat bath, which contributes to the discontinuity at arbitrary energy for σ , as discussed above. If we include them, the structure of the spectral function might be significantly modified. Their effects on the spectral function cannot be taken into account till we extend the calculation including two-loop self-energies.

In this paper, we take a step forward in the calculation of two-loop self-energy diagrams, i.e. we evaluate the thermal sunset diagram for scalar field theories. After giving a brief review of the real time formalism [2-14] in the second section, which we use for the calculation of diagrams, we first examine the bubble diagram, a one-loop diagram which appears as a subdiagram of the sunset diagram, at finite temperature in the third section. Then, we discuss the structure of the discontinuous part of the thermal sunset diagram in the fourth section and explain how we calculate the sunset diagram in the fifth section. Using our result for this diagram, we study the effects of the diagram on the spectral function of σ at finite temperature in $\mathcal{O}(4)$ linear sigma model in the sixth section. Finally we summarize the paper in the seventh section.

II. BRIEF REVIEW OF THE REAL TIME FORMALISM

For the calculations of thermal Feynman diagrams we adopt the real time formalism throughout this paper. We briefly review the formalism in this section.

In the real time formalism propagators are given by 2×2 matrices. The 4-components of the free propagator of a scalar particle with mass m are given by [14]

$$i\Delta_{11}^F(k; m) = \frac{i}{k^2 - m^2 + i\eta} + n(k_0)2\pi\delta(k^2 - m^2), \quad (\text{II.1})$$

$$i\Delta_{12}^F(k; m) = e^{\sigma k_0}[n(k_0) + \theta(-k_0)]2\pi\delta(k^2 - m^2), \quad (\text{II.2})$$

$$i\Delta_{21}^F(k; m) = e^{-\sigma k_0}[n(k_0) + \theta(k_0)]2\pi\delta(k^2 - m^2), \quad (\text{II.3})$$

$$i\Delta_{22}^F(k; m) = \frac{-i}{k^2 - m^2 - i\eta} + n(k_0)2\pi\delta(k^2 - m^2), \quad (\text{II.4})$$

where $n(k_0)$ is the Bose-Einstein distribution function at temperature $T \equiv 1/\beta$:

$$n(k_0) = \frac{1}{\exp(\beta|k_0|) - 1}. \quad (\text{II.5})$$

Off-diagonal elements depend on a free parameter σ . In this paper we make the symmetrical choice $\sigma = \beta/2$, leading to

$$i\Delta_{12}^F(k; m) = i\Delta_{21}^F(k; m) = e^{\beta|k_0|/2}n(k_0)2\pi\delta(k^2 - m^2). \quad (\text{II.6})$$

We denote the matrix of the full propagator by

$$\tilde{\Delta}(k; m) = \begin{pmatrix} \Delta_{11}(k; m) & \Delta_{12}(k; m) \\ \Delta_{21}(k; m) & \Delta_{22}(k; m) \end{pmatrix}. \quad (\text{II.7})$$

Each component is the solution of the Schwinger-Dyson equation:

$$\Delta_{ab}(k; m) = \Delta_{ab}^F(k; m) + \Delta_{ac}^F(k; m)\Pi_{cd}(k)\Delta_{db}(k; m), \quad (\text{II.8})$$

where $\Pi_{cd}(k)$ is the self-energy.

The following matrix

$$U(k) = \begin{pmatrix} \sqrt{1+n(k_0)} & \sqrt{n(k_0)} \\ \sqrt{n(k_0)} & \sqrt{1+n(k_0)} \end{pmatrix}, \quad (\text{II.9})$$

‘diagonalizes’ the free propagator:

$$U(k)^{-1} \begin{pmatrix} \Delta_{11}^F(k; m) & \Delta_{12}^F(k; m) \\ \Delta_{21}^F(k; m) & \Delta_{22}^F(k; m) \end{pmatrix} U(k)^{-1} = \begin{pmatrix} \Delta_0^F(k; m) & 0 \\ 0 & -\Delta_0^F(k; m)^* \end{pmatrix}, \quad (\text{II.10})$$

where $\Delta_0^F(k; m)$ is the Feynman propagator at $T = 0$

$$\Delta_0^F(k; m) = \frac{1}{k^2 - m^2 + i\eta}. \quad (\text{II.11})$$

It is known that $U(k)$ also diagonalizes the full propagator [14] as well as $\Pi_{ab}(k)$

$$\Pi_{ab}(k) = (U(k)^{-1})_{ac} \begin{pmatrix} \bar{\Pi}(k) & 0 \\ 0 & -\bar{\Pi}(k)^* \end{pmatrix}_{cd} (U(k)^{-1})_{db}. \quad (\text{II.12})$$

This matrix equation gives relations between matrix elements:

$$\text{Re}\bar{\Pi}(k) = \text{Re}\Pi_{11}(k), \quad (\text{II.13})$$

$$\text{Im}\bar{\Pi}(k) = \tanh(\beta|k_0|/2)\text{Im}\Pi_{11}(k), \quad (\text{II.14})$$

$$\text{Im}\bar{\Pi}(k) = i \sinh(\beta|k_0|/2)\Pi_{12}(k). \quad (\text{II.15})$$

Let us next find the expression of the spectral function. Δ_{11} has the following spectral representation:

$$\Delta_{11}(k; m) = \int d\omega^2 \rho(\omega, \mathbf{k}) \Delta_{11}^F(k_0, \omega), \quad (\text{II.16})$$

where we denote the argument of Δ_{11}^F by k_0 and $\omega \equiv \sqrt{\mathbf{k}^2 + m^2}$ instead of k and m . One can prove that, if Δ_{11} is given in Eq.(II.16), the Green function

$$\Delta(t, \mathbf{x}) = \frac{i}{(2\pi)^4} \int d^4k e^{ik \cdot x} \Delta_{11}(k; m) \quad (\text{II.17})$$

obeys the Kubo-Martin-Schwinger (KMS) condition [15]. From Eq.(II.16) we obtain

$$\rho(k) = -\frac{1}{\pi} \tanh(\beta|k_0|/2) \text{Im} \Delta_{11}(k; m). \quad (\text{II.18})$$

Our next task is thus to find the expression of $\text{Im} \Delta_{11}(k; m)$. Denoting the diagonalized full propagator by

$$U(k)^{-1} \tilde{\Delta}(k; m) U(k)^{-1} = \begin{pmatrix} \Delta(k; m) & 0 \\ 0 & -\Delta(k; m)^* \end{pmatrix}, \quad (\text{II.19})$$

we obtain

$$\begin{aligned} \tilde{\Delta} &= U(k) \begin{pmatrix} \Delta(k; m) & 0 \\ 0 & -\Delta(k; m)^* \end{pmatrix} U(k) \\ &= \begin{pmatrix} [1 + n(k_0)]\Delta(k; m) - n(k_0)\Delta(k; m)^* & \sqrt{n(k_0)[1 + n(k_0)]}[\Delta(k; m) - \Delta(k; m)^*] \\ \sqrt{n(k_0)[1 + n(k_0)]}[\Delta(k; m) - \Delta(k; m)^*] & -[1 + n(k_0)]\Delta(k; m)^* + n(k_0)\Delta(k; m) \end{pmatrix}. \end{aligned} \quad (\text{II.20})$$

Taking the (1, 1)-components in the both sides of the above equation yields

$$\text{Im} \Delta_{11}(k; m) = \coth(\beta|k_0|/2) \text{Im} \Delta(k; m). \quad (\text{II.21})$$

The expression for $\Delta(k; m)$ can be found in the following manner. In Eq.(II.8), iteratively using Eq.(II.8) itself in the right hand side and diagonalizing, we obtain

$$\begin{aligned} U(k)^{-1} \tilde{\Delta}(k; m) U(k)^{-1} &= \begin{pmatrix} \Delta_0^F(k; m) & 0 \\ 0 & -\Delta_0^F(k; m)^* \end{pmatrix} \\ &+ \begin{pmatrix} \Delta_0^F(k; m) & 0 \\ 0 & -\Delta_0^F(k; m)^* \end{pmatrix} \begin{pmatrix} \bar{\Pi}(k) & 0 \\ 0 & -\bar{\Pi}(k)^* \end{pmatrix} \begin{pmatrix} \Delta_0^F(k; m) & 0 \\ 0 & -\Delta_0^F(k; m)^* \end{pmatrix} + \dots \end{aligned} \quad (\text{II.22})$$

The (1,1) component of this equation gives

$$\begin{aligned}
\Delta(k; m) &= (U(k)^{-1} \tilde{\Delta}(k; m) U(k)^{-1})_{11} \\
&= \Delta_0^F(k; m) + \Delta_0^F(k; m) \bar{\Pi}(k) \Delta_0^F(k; m) + \dots \\
&= \frac{1}{k^2 - m^2 - \bar{\Pi}(k)}.
\end{aligned} \tag{II.23}$$

Therefore, from Eqs.(II.18), (II.21) and (II.23), we obtain the desired expression of the spectral function:

$$\rho(k) = -\frac{1}{\pi} \frac{\text{Im} \bar{\Pi}(k)}{[k^2 - m^2 - \text{Re} \bar{\Pi}(k)]^2 + [\text{Im} \bar{\Pi}(k)]^2}. \tag{II.24}$$

Thus the spectral function can be written only with one component of the self-energies while all the components enter $\Delta_{11}(k; m)$ (see Eq.(II.8)).

III. BUBBLE DIAGRAM

In this section we examine the ‘‘bubble’’ diagram, which is a one-loop diagram shown in Fig.2. The bubble diagram appears as a subdiagram of the sunset diagram and therefore we need the expression of the former in the calculation of the latter.

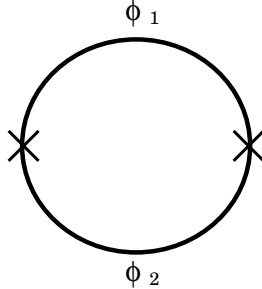


FIG. 2: ‘‘Bubble’’ diagram.

Among the 4-components of the bubble diagram we need only the (1,1) component since the sunset diagram does not have any internal vertices. The (1,1) component of the bubble diagram for scalar particles is given by

$$\mathcal{I}_{\text{bub}}(p; m_1, m_2)_{11} = \int \frac{d^4 k}{(2\pi)^4} i \Delta_{11}^F(p+k; m_1) i \Delta_{11}^F(k; m_2). \tag{III.25}$$

Eq.(III.25) can be expressed as the sum of terms with different numbers of Bose-Einstein factors, n :

$$\mathcal{I}_{\text{bub}}(p; m_1, m_2)_{11} = I^{(2)}(p^2; m_1, m_2) + (F^{(2)}(p; m_1, m_2) + (1 \leftrightarrow 2)) + F^{(3)}(p; m_1, m_2). \tag{III.26}$$

Each term in the right hand side is respectively given by

$$I^{(2)}(p^2; m_1, m_2) = \int \frac{d^4k}{(2\pi)^4} \frac{i}{(p+k)^2 - m_1^2 + i\eta} \frac{i}{k^2 - m_2^2 + i\eta}, \quad (\text{III.27})$$

$$F^{(2)}(p; m_1, m_2) = \int \frac{d^4k}{(2\pi)^4} \frac{i}{(p+k)^2 - m_1^2 + i\eta} n(k_0) 2\pi \delta(k^2 - m_2^2), \quad (\text{III.28})$$

$$F^{(3)}(p; m_1, m_2) = \int \frac{d^4k}{(2\pi)^4} n(p_0 + k_0) 2\pi \delta((p+k)^2 - m_1^2) n(k_0) 2\pi \delta(k^2 - m_2^2). \quad (\text{III.29})$$

Let us carry out the integration in the above equations. The T -independent part $I^{(2)}$ is given in textbooks [16]. In d -dimension it is given by

$$I^{(2)}(p^2; m_1, m_2) = \frac{i}{16\pi^2} \left(-\frac{1}{\bar{\epsilon}} + x_+ \ln \frac{m_1^2}{\kappa^2} - x_- \ln \frac{m_2^2}{\kappa^2} - 2 - I \right), \quad (\text{III.30})$$

where κ is the renormalization point and $\frac{1}{\bar{\epsilon}}$ and x_{\pm} are

$$\frac{1}{\bar{\epsilon}} \equiv \frac{1}{\epsilon} - \gamma + \ln 4\pi \quad (\epsilon = (4-d)/2, \quad \gamma : \text{Euler constant}), \quad (\text{III.31})$$

$$x_{\pm} \equiv \pm \frac{1}{2} + \frac{m_1^2 - m_2^2}{2p^2}. \quad (\text{III.32})$$

I is given by

$$I = \begin{cases} \sqrt{C} \left[\ln \frac{(x_+ - \sqrt{C})(x_- + \sqrt{C})}{(x_- - \sqrt{C})(x_+ + \sqrt{C})} + i2\pi \right] & \text{for } p^2 > (m_1 + m_2)^2, \\ -2\sqrt{D} \left[\arctan \frac{x_+}{\sqrt{D}} - \arctan \frac{x_-}{\sqrt{D}} \right] & \text{for } (m_1 - m_2)^2 < p^2 < (m_1 + m_2)^2, \\ \sqrt{C} \ln \frac{(\sqrt{C} - x_+)(\sqrt{C} + x_-)}{(\sqrt{C} - x_-)(\sqrt{C} + x_+)} & \text{for } p^2 < (m_1 - m_2)^2, \end{cases} \quad (\text{III.33})$$

where C and D are

$$C \equiv \frac{1}{4} \left[1 - \frac{(m_1 + m_2)^2}{p^2} \right] \left[1 - \frac{(m_1 - m_2)^2}{p^2} \right], \quad D \equiv -C. \quad (\text{III.34})$$

We see from Eqs.(III.27) and (III.33) that the discontinuous part, $\text{Im}iI^{(2)}$, is non-vanishing for $p^2 > (m_1 + m_2)^2$.

The divergent part in Eq.(III.27) is renormalized by applying a counter term to the Lagrangian. The finite part is determined in such a way that the resultant self-energy satisfies a proper normalization condition.

Let us next turn to the T -dependent part, $F^{(2)}$ and $F^{(3)}$. We first discuss their discontinuous parts. As shown in Appendix A the discontinuous part of $F^{(2)}(p; m_1, m_2)$ is given analytically as follows:

1. For $p^2 > (m_1 + m_2)^2$ or $0 < p^2 < (m_1 - m_2)^2$,

$$\text{Im}iF^{(2)}(p; m_1, m_2) = \frac{1}{16\pi|\mathbf{p}|} \frac{1}{\beta} \ln \left| \frac{1 - e^{-\beta\omega_+}}{1 - e^{-\beta\omega_-}} \right|. \quad (\text{III.35})$$

2. For $(m_1 - m_2)^2 < p^2 < (m_1 + m_2)^2$,

$$\text{Im}iF^{(2)}(p; m_1, m_2) = 0. \quad (\text{III.36})$$

3. For $p^2 < 0$,

$$\text{Im}iF^{(2)}(p; m_1, m_2) = \frac{1}{16\pi|\mathbf{p}|} \frac{-1}{\beta} \ln |(1 - e^{-\beta\omega_+})(1 - e^{-\beta\omega_-})|. \quad (\text{III.37})$$

Here,

$$\omega_{\pm} = \frac{1}{2} \left| \sqrt{\left(1 + \frac{m_2^2 - m_1^2}{p^2}\right)^2} |p_0| \pm \sqrt{\left[1 - \frac{(m_2 + m_1)^2}{p^2}\right] \left[1 - \frac{(m_1 - m_2)^2}{p^2}\right]} |\mathbf{p}| \right|. \quad (\text{III.38})$$

$F^{(3)}$ has only discontinuous part. Its calculation can be done in a way similar to that for $\text{Im}iF^{(2)}(p; m_1, m_2)$. We show the final results:

1. For $p^2 > (m_1 + m_2)^2$,

$$F^{(3)}(p; m_1, m_2) = \frac{1}{8\pi|\mathbf{p}|} \frac{1}{\beta} \frac{1}{e^{\beta|p_0|} - 1} \ln \left| \frac{1 - e^{-\beta\omega_+} e^{\beta(|p_0| - \omega_-)} - 1}{1 - e^{-\beta\omega_-} e^{\beta(|p_0| - \omega_+)} - 1} \right|. \quad (\text{III.39})$$

2. For $(m_1 - m_2)^2 < p^2 < (m_1 + m_2)^2$,

$$F^{(3)}(p; m_1, m_2) = 0. \quad (\text{III.40})$$

3. For $0 < p^2 < (m_1 - m_2)^2$,

$$F^{(3)}(p; m_1, m_2) = \frac{1}{8\pi|\mathbf{p}|} \frac{1}{\beta} \cdot \frac{1}{e^{\beta|p_0|} - 1} \times \left[\ln \left| \frac{1 - e^{-\beta\omega_+}}{1 - e^{-\beta\omega_-}} \right| - e^{\beta|p_0|} \ln \left| \frac{1 - e^{-\beta(|p_0| + \omega_+)}}{1 - e^{-\beta(|p_0| + \omega_-)}} \right| \right]. \quad (\text{III.41})$$

4. For $p^2 < 0$,

$$F^{(3)}(p; m_1, m_2) = \frac{1}{8\pi|\mathbf{p}|} \frac{1}{\beta} \left\{ \frac{1}{e^{-\beta|p_0|} - 1} [-\ln|1 - e^{-\beta\omega_+}| + e^{-\beta|p_0|} \ln|1 - e^{-\beta(\omega_+ - |p_0|)}|] \right. \\ \left. + \frac{1}{e^{\beta|p_0|} - 1} [-\ln|1 - e^{-\beta\omega_-}| + e^{\beta|p_0|} \ln|1 - e^{-\beta(\omega_- + |p_0|)}|] \right\}. \quad (\text{III.42})$$

In the above equations ω_{\pm} are given by Eq.(III.38) with m_1 and m_2 replaced by $\max\{m_1, m_2\}$ and $\min\{m_1, m_2\}$, respectively, since $F^{(3)}(p; m_1, m_2)$ is symmetric with respect to m_1 and m_2 by definition.

It should be noted that the T -dependent part has two cuts in the complex p^2 plane: one starts from $p^2 = (m_1 + m_2)^2$ to the right along the real axis and the other from $p^2 = (m_1 - m_2)^2$ to the left.

Let us next discuss the continuous part of $F^{(2)}$, which is

$$\text{Re}iF^{(2)}(p; m_1, m_2) = - \int \frac{d^4k}{(2\pi)^4} \mathcal{P} \frac{1}{(p+k)^2 - m_1^2} n(k_0) 2\pi\delta(k^2 - m_2^2), \quad (\text{III.43})$$

where \mathcal{P} stands for the prescription of Cauchy's principal value. After integration over k_0 and angle, we can express Eq.(III.43) as a one-dimensional integral:

$$\begin{aligned} & \text{Re}iF^{(2)}(p; m_1, m_2) \\ &= \frac{1}{16\pi^2|\mathbf{p}|} \int_{m_2}^{\infty} d\omega n(\omega) \\ &\times \mathcal{P} \ln \left| \frac{(p^2 + 2p_0\omega - 2|\mathbf{p}|\sqrt{\omega^2 - m_2^2} + m_2^2 - m_1^2)(p^2 - 2p_0\omega - 2|\mathbf{p}|\sqrt{\omega^2 - m_2^2} + m_2^2 - m_1^2)}{(p^2 + 2p_0\omega + 2|\mathbf{p}|\sqrt{\omega^2 - m_2^2} + m_2^2 - m_1^2)(p^2 - 2p_0\omega + 2|\mathbf{p}|\sqrt{\omega^2 - m_2^2} + m_2^2 - m_1^2)} \right|, \end{aligned} \quad (\text{III.44})$$

whose integration will be carried out numerically.

IV. STRUCTURE OF THE DISCONTINUOUS PART OF THE SUNSET DIAGRAM

Before proceeding to the calculation of the thermal sunset diagram, we study the structure of the discontinuous part of the diagram. In ref.[18], Weldon analyzed the discontinuous part of the bubble diagram. We will generalize it for the sunset diagram. For this purpose it is convenient to use Eq.(II.15) [17], namely

$$\text{Im}i\bar{\mathcal{I}}_{\text{sun}}(k; m_1, m_2, m_3) = i \sinh(\beta|k_0|/2) i\mathcal{I}_{\text{sun}}(k; m_1, m_2, m_3)_{12}. \quad (\text{IV.45})$$

Here $\bar{\mathcal{I}}_{\text{sun}}(k; m_1, m_2, m_3)$ is the (1, 1) component of the diagonalized self-energy matrix for the sunset diagram. We note that the self-energy which actually enters spectral functions is diagonalized one (see Eq.(II.24)). $\mathcal{I}_{\text{sun}}(k; m_1, m_2, m_3)_{12}$ is the (1, 2) component of the sunset diagram, which is given by the following integral:

$$i\mathcal{I}_{\text{sun}}(k; m_1, m_2, m_3)_{12} = \int \frac{d^4p}{(2\pi)^4} i\Delta_{12}^F(p; m_1) i\mathcal{I}_{\text{bub}}(k-p; m_2, m_3)_{12}. \quad (\text{IV.46})$$

For $i\Delta_{12}^F(p; m_1)$ it is convenient to use another form:

$$\begin{aligned} i\Delta_{12}^F(p; m_1) &= e^{\beta p_0/2} f(p_0) \epsilon(p_0) 2\pi \delta(p^2 - m_1^2), \\ f(p_0) &= \frac{1}{e^{\beta p_0} - 1}. \end{aligned} \quad (\text{IV.47})$$

$i\mathcal{I}_{\text{bub}}(p; m_1, m_2)_{12}$ denotes the (1, 2) component of the bubble diagram:

$$i\mathcal{I}_{\text{bub}}(k - p; m_2, m_3)_{12} = i \int \frac{d^4 q}{(2\pi)^4} i\Delta_{12}^F(q; m_2) i\Delta_{12}^F(k - p - q; m_3). \quad (\text{IV.48})$$

One can reduce this equation to

$$\begin{aligned} &i\mathcal{I}_{\text{bub}}(p; m_1, m_2)_{12} \\ &= i e^{\beta(k_0 - p_0)/2} f(k_0 - p_0) \\ &\quad \times \int \frac{d^4 q}{(2\pi)^2} \frac{1}{4E_2 E_3} \{ (1 + n_2 + n_3) [\delta(k_0 - p_0 - E_2 - E_3) - \delta(k_0 - p_0 - E_2 + E_3)] \\ &\quad - (n_2 - n_3) [\delta(k_0 - p_0 - E_2 + E_3) - \delta(k_0 - p_0 + E_2 - E_3)] \}, \end{aligned} \quad (\text{IV.49})$$

where $E_2 = \sqrt{|\mathbf{q}|^2 + m_2^2}$ and $E_3 = \sqrt{|\mathbf{k} - \mathbf{p} - \mathbf{q}|^2 + m_3^2}$. We also define $E_1 = \sqrt{|\mathbf{p}|^2 + m_1^2}$ for later use. n_i is the Bose-Einstein factor defined by $n_i = n(E_i)$. Using Eq.(IV.45) and Eq.(IV.46) in which Eq.(IV.49) is substituted yields

$$\begin{aligned} &\text{Im} i\bar{\mathcal{I}}_{\text{sun}}(k; m_1, m_2, m_3) \\ &= -\pi \epsilon(k_0) \int \frac{d^3 p}{(2\pi)^3} \int \frac{d^3 q}{(2\pi)^3} \frac{1}{8E_1 E_2 E_3} \\ &\quad \times \{ ((1 + n_1)(1 + n_2)(1 + n_3) - n_1 n_2 n_3) \delta(k_0 - E_1 - E_2 - E_3) \\ &\quad + (n_1 n_2 n_3 - (1 + n_1)(1 + n_2)(1 + n_3)) \delta(k_0 + E_1 + E_2 + E_3) \\ &\quad + [(n_2 n_3(1 + n_1) - n_1(1 + n_2)(1 + n_3)) \delta(k_0 - E_1 + E_2 + E_3) \\ &\quad + (n_1(1 + n_2)(1 + n_3) - n_2 n_3(1 + n_1)) \delta(k_0 + E_1 - E_2 - E_3) + (\text{permutations})] \}. \end{aligned} \quad (\text{IV.50})$$

In this equation ‘‘permutations’’ stands for the terms obtained by permuting the particle labels of the third and the fourth terms.

Let us now consider the physical content of Eq.(IV.50). The first term in Eq.(IV.50) may be interpreted as the probability for the decay $\Phi \rightarrow \phi_1 \phi_2 \phi_3$ with the statistical weight $(1 + n_1)(1 + n_2)(1 + n_3)$ for stimulated emission minus the probability for the creation $\phi_1 \phi_2 \phi_3 \rightarrow \Phi$ with the weight $n_1 n_2 n_3$ for absorption. The second term is the anti-particle counter part of the first term. The third term represents the probability for $\Phi \bar{\phi}_2 \bar{\phi}_3 \rightarrow \phi_1$ with the weight $n_2 n_3(1 + n_1)$ minus that for $\phi_1 \rightarrow \Phi \bar{\phi}_2 \bar{\phi}_3$ with the weight $n_1(1 + n_2)(1 + n_3)$. Here

$\bar{\phi}_i$ stands for the anti-particle of ϕ_i . The fourth term is the anti-particle counter part of the third term. It represents the probability for $\Phi\bar{\phi}_1 \rightarrow \phi_2\phi_3$ with the weight $n_1(1+n_2)(1+n_3)$ minus that for $\phi_2\phi_3 \rightarrow \Phi\bar{\phi}_1$ with the weight $n_2n_3(1+n_1)$. All processes are shown in Fig.3.

We next find the region of k^2 where the physical processes contained in Eq.(IV.50) are possible, which is equivalent to looking for the condition under which the integral over q in Eq.(IV.50) survives. For the first and the second terms in Eq.(IV.50) to be non-vanishing, k^2 must satisfy the condition $k^2 > (m_1 + M_{23})^2$, where M_{23} is the invariant mass of ϕ_2 and ϕ_3 . Therefore, the processes in Fig.3 (a), (b), (c) and (d) are possible for $k^2 > (m_1 + m_2 + m_3)^2$ since $M_{23} > m_2 + m_3$. The third and the fourth terms survive when $k^2 < (m_1 - M_{23})^2$. The processes in Fig.3 (e), (f), (g) and (h), therefore, take place at arbitrary k^2 . This is reasonable since the processes in Fig.3 (g) and (h) are scattering ones and since those in Fig.3 (e) and (f) can be also regarded as scattering by interpreting the incoming Φ in (e) as an outgoing anti- Φ and by doing the outgoing Φ in (f) as an incoming anti- Φ . Accordingly, the discontinuous part of the sunset diagram is non-vanishing for arbitrary k^2 , which is a remarkable feature of the thermal self-energy at and beyond two-loop order.

V. CALCULATION OF THE THERMAL SUNSET DIAGRAM

In this section, we explain how to calculate the thermal sunset diagram by reducing it to an expression written in terms of the bubble diagram previously obtained.

The (1,1) component of the sunset diagram shown in Fig.1 is given by

$$\mathcal{I}_{\text{sun}}(k; m_1, m_2, m_3)_{11} = \int \frac{d^4p}{(2\pi)^4} i\Delta_{11}^F(p; m_1) \int \frac{d^4q}{(2\pi)^4} i\Delta_{11}^F(q; m_2) i\Delta_{11}^F(k-p-q; m_3). \quad (\text{V.51})$$

We decompose Eq.(V.51) into terms without and with Bose-Einstein factors, which we denote by $\mathcal{I}_{\text{sun}}^{\text{vac}}(k^2; m_1, m_2, m_3)_{11}$ and $\mathcal{I}_{\text{sun}}^{\text{th}}(k; m_1, m_2, m_3)_{11}$, respectively:

$$\mathcal{I}_{\text{sun}}(k; m_1, m_2, m_3)_{11} = \mathcal{I}_{\text{sun}}^{\text{vac}}(k^2; m_1, m_2, m_3)_{11} + \mathcal{I}_{\text{sun}}^{\text{th}}(k; m_1, m_2, m_3)_{11}. \quad (\text{V.52})$$

They are given by

$$\begin{aligned} \mathcal{I}_{\text{sun}}^{\text{vac}}(k^2; m_1, m_2, m_3)_{11} &= \int \frac{d^4p}{(2\pi)^4} \frac{i}{p^2 - m_1^2 + i\eta} I^{(2)}((k-p)^2; m_2, m_3), \\ \mathcal{I}_{\text{sun}}^{\text{th}}(k; m_1, m_2, m_3)_{11} &= \int \frac{d^4p}{(2\pi)^4} \frac{i}{p^2 - m_1^2 + i\eta} \\ &\quad \times \left[(F^{(2)}(k-p; m_2, m_3) + (2 \leftrightarrow 3)) + F^{(3)}(k-p; m_2, m_3) \right] \end{aligned} \quad (\text{V.53})$$

$$\begin{aligned}
& + \int \frac{d^4 p}{(2\pi)^4} n(p_0) 2\pi \delta(p^2 - m_1^2) [I^{(2)}((k-p)^2; m_2, m_3) \\
& \quad + (F^{(2)}(k-p; m_2, m_3) + (2 \leftrightarrow 3)) + F^{(3)}(k-p; m_2, m_3)].
\end{aligned} \tag{V.54}$$

Here we have expressed the second integral in Eq.(V.51) in terms of $I^{(2)}$, $F^{(2)}$ and $F^{(3)}$. The T -independent part, Eq.(V.53), has a subdivergence coming from the nested bubble diagram and a two-loop overall divergence. On the other hand, T -dependent part, Eq.(V.54), has only a subdivergence, which can be removed by carrying out renormalization at one-loop level. Hereafter, $I^{(2)}$ expresses that with the divergence removed. We calculate Eqs.(V.53) and (V.54) separately.

A. T -independent part

The T -independent part of sunset type diagrams has been calculated by several authors [19-22] so far. In this paper we calculate its finite part using a dispersion relation.

We first find the discontinuous part of $\mathcal{I}_{\text{sun}}^{\text{vac}}(k^2; m_1, m_2, m_3)_{11}$ and then compute the finite continuous part using the obtained discontinuous part, *via* the twice-subtracted dispersion relation.

In order to calculate the discontinuous part of $\mathcal{I}_{\text{sun}}^{\text{vac}}(k^2; m_1, m_2, m_3)_{11}$, we substitute a dispersion relation for $iI^{(2)}((k-p)^2; m_2, m_3)$:

$$iI^{(2)}((k-p)^2; m_2, m_3) = \frac{1}{\pi} \int_{(m_2+m_3)^2}^{\infty} dM^2 \frac{\text{Im}iI^{(2)}(M^2; m_2, m_3)}{M^2 - (k-p)^2 - i\eta}, \tag{V.55}$$

into Eq.(V.53). Then, we obtain

$$\begin{aligned}
\mathcal{I}_{\text{sun}}^{\text{vac}}(k^2; m_1, m_2, m_3)_{11} &= \frac{1}{\pi} \int_{(m_2+m_3)^2}^{\infty} dM^2 \text{Im}iI^{(2)}(M^2; m_2, m_3) \\
&\quad \times \int \frac{d^4 p}{(2\pi)^4} \frac{i}{p^2 - m_1^2 + i\eta} \frac{i}{(k-p)^2 - M^2 + i\eta} \\
&= \frac{1}{\pi} \int_{(m_2+m_3)^2}^{\infty} dM^2 \text{Im}iI^{(2)}(M^2; m_2, m_3) I^{(2)}(k^2; m_1, M).
\end{aligned} \tag{V.56}$$

We take the discontinuous part of this equation:

$$\text{Im}i\mathcal{I}_{\text{sun}}^{\text{vac}}(k^2; m_1, m_2, m_3)_{11} = \frac{1}{\pi} \int_{(m_2+m_3)^2}^{\infty} dM^2 \text{Im}iI^{(2)}(M^2; m_2, m_3) \text{Im}iI^{(2)}(k^2; m_1, M). \tag{V.57}$$

Using the expression for $\text{Im}iI^{(2)}(p^2; m, m_2)$ we can easily evaluate Eq.(V.57) numerically.

Next we turn to the continuous part. The continuous part of Eq.(V.53) is divergent. Therefore one needs corresponding counter terms in the Lagrangian. The second and third diagrams of Fig.4 appear at two-loop order, which cancel the divergences in the bare sunset diagram, the first diagram of Fig.4. In this paper, we do not explicitly go through the renormalization procedure but concentrate on the finite part.

In order to calculate the finite part, we use the twice-subtracted dispersion relation:

$$\begin{aligned}
& \text{Re}i\tilde{\mathcal{I}}_{\text{sun}}^{\text{vac}}(k^2; m_1, m_2, m_3)_{11} \\
\equiv & \text{Re} \left\{ i\mathcal{I}_{\text{sun}}^{\text{vac}}(k^2; m_1, m_2, m_3)_{11} - i\mathcal{I}_{\text{sun}}^{\text{vac}}(0; m_1, m_2, m_3)_{11} - k^2 \left[\frac{\partial}{\partial k^2} i\mathcal{I}_{\text{sun}}^{\text{vac}}(k^2; m_1, m_2, m_3)_{11} \right]_{k^2=0} \right\} \\
= & \frac{k^4}{\pi} \int_{(m_1+m_2+m_3)^2}^{\infty} dM^2 \mathcal{P} \frac{\text{Im}i\mathcal{I}_{\text{sunset}}^{\text{vac}}(M^2; m_1, m_2, m_3)}{M^4(M^2 - k^2)}. \tag{V.58}
\end{aligned}$$

The second and the third terms in the left hand side are divergent and have to be renormalized but the right hand side is finite and remain unchanged by renormalization. Using the results for $\text{Im}i\mathcal{I}_{\text{sun}}^{\text{vac}}(M^2; m_1, m_2, m_3)$ we can easily evaluate Eq.(V.58) numerically. After $\text{Re}i\tilde{\mathcal{I}}_{\text{sun}}^{\text{vac}}(m_{\text{phys}}^2; m_1, m_2, m_3)_{11}$ is subtracted, Eq.(V.58) coincides with that in modified minimal subtraction scheme up to an irrelevant overall factor.

B. T -dependent part

We rewrite the integrand of the first term in the T -dependent part Eq.(V.54) so that it becomes the same form as that in the second term, *i.e.* (a delta function) \times (some functions). This can be done by recombining the two factors in the integrand of $F^{(2)}(k-p; m_2, m_3) + (2 \leftrightarrow 3)$ and $F^{(3)}(k-p; m_2, m_3)$, T -independent part and T -dependent part of $i\Delta_{11}^F$. The result is as follows:

$$\begin{aligned}
& \mathcal{I}_{\text{sun}}^{\text{th}}(k; m_1, m_2, m_3)_{11} \\
= & \int \frac{d^4p}{(2\pi)^4} \left\{ n(p_0) 2\pi \delta(p^2 - m_1^2) [I^{(2)}(k-p; m_2, m_3) + (F^{(2)}(k-p; m_2, m_3) + (2 \leftrightarrow 3)) \right. \\
& \left. + F^{(3)}(k-p; m_2, m_3)] \right. \\
& \left. + n(p_0) 2\pi \delta(p^2 - m_2^2) [I^{(2)}(k-p; m_1, m_3) + F^{(2)}(k-p; m_1, m_3)] \right. \\
& \left. + n(p_0) 2\pi \delta(p^2 - m_3^2) I^{(2)}(k-p; m_1, m_2) \right\}. \tag{V.59}
\end{aligned}$$

When we put $k = (k_0, \mathbf{0})$, Eq.(V.59) is reduced to

$$\mathcal{I}_{\text{sun}}^{\text{th}}(k_0, \mathbf{0}; m_1, m_2, m_3)_{11}$$

$$\begin{aligned}
&= \frac{1}{4\pi^2} \sum_{\tau=\pm} \left\{ \int_{m_1}^{\infty} d\omega n(\omega) \sqrt{\omega^2 - m_1^2} \left[I^{(2)}(k_0 + \tau\omega, \sqrt{\omega^2 - m_1^2}; m_2, m_3) \right. \right. \\
&\quad + \left(F^{(2)}(k_0 + \tau\omega, \sqrt{\omega^2 - m_1^2}; m_2, m_3) + (2 \leftrightarrow 3) \right) \\
&\quad \left. + F^{(3)}(k_0 + \tau\omega, \sqrt{\omega^2 - m_1^2}; m_2, m_3) \right] \\
&\quad + \int_{m_2}^{\infty} d\omega n(\omega) \sqrt{\omega^2 - m_2^2} \left[I^{(2)}(k_0 + \tau\omega, \sqrt{\omega^2 - m_2^2}; m_1, m_3) \right. \\
&\quad \left. + F^{(2)}(k_0 + \tau\omega, \sqrt{\omega^2 - m_2^2}; m_1, m_3) \right] \\
&\quad \left. + \int_{m_3}^{\infty} d\omega n(\omega) \sqrt{\omega^2 - m_3^2} \cdot I^{(2)}(k_0 + \tau\omega, \sqrt{\omega^2 - m_3^2}; m_1, m_2) \right\}, \quad (\text{V.60})
\end{aligned}$$

Using the expressions of $I^{(2)}$, $F^{(2)}$ and $F^{(3)}$ obtained in the previous section, we can evaluate the continuous and discontinuous parts of Eq.(V.60) numerically.

VI. CONTRIBUTION OF THE THERMAL SUNSET DIAGRAM TO THE SPECTRAL FUNCTION OF THE SIGMA MESON AT FINITE TEMPERATURE

The purpose of this section is to see how two-loop diagrams affect observables by evaluating the contribution of the thermal sunset diagram to σ spectral function at finite temperature in the $\mathcal{O}(4)$ linear sigma model.

It is known that naive perturbation theory breaks down at $T \neq 0$ and that resummation of higher orders is necessary [23,24]. We adopt here a resummation technique called optimized perturbation theory (OPT) [1]. We first briefly review the procedure of OPT applied to $\mathcal{O}(4)$ linear sigma model. The original linear sigma model Lagrangian is as follows:

$$\mathcal{L} = \frac{1}{2} [(\partial_\mu \phi_i)^2 - \mu^2 \phi_i^2] - \frac{\lambda}{4!} (\phi_i^2)^2 + h\phi_0 + \text{counter terms}, \quad (\text{VI.61})$$

where $\phi_i = (\sigma, \vec{\pi})$ and $h\phi_0$ being the explicitly symmetry breaking term. For the renormalized couplings μ^2 , λ and h and the renormalization point κ we use the values determined in [1]: $\mu^2 = -(283 \text{ MeV})^2$, $\lambda = 73.0$, $h = (123 \text{ MeV})^3$, $\kappa = 255 \text{ MeV}$.

In OPT one adds and subtracts a new mass term with the mass m to the Lagrangian. Thus, we have

$$\mathcal{L} = \frac{1}{2} [(\partial_\mu \phi_i)^2 - m^2 \phi_i^2] + \frac{1}{2} \chi \phi_i^2 - \frac{\lambda}{4!} (\phi_i^2)^2 + h\phi_0 + (\text{counter term}), \quad (\text{VI.62})$$

where $\chi \equiv m^2 - \mu^2$. The idea of OPT is reorganization of perturbation theory: one treats the added one as a tree-level mass term while the subtracted one as perturbation.

When the spontaneous symmetry breaking takes place, tree level masses of π and σ read, respectively,

$$m_{0\pi}^2 = m^2 + \frac{\lambda}{6}\xi^2, \quad m_{0\sigma}^2 = m^2 + \frac{\lambda}{2}\xi^2, \quad (\text{VI.63})$$

where ξ is the vacuum expectation value of σ and determined by the stationary condition for the thermal effective action $V(\xi, T, m^2)$ [1]:

$$\frac{\partial V(\xi, T, m^2)}{\partial \xi} = 0. \quad (\text{VI.64})$$

Note that the derivative with respect to ξ does not act on m^2 .

If Green's functions are calculated in all orders in OPT, they should not depend on the arbitrary mass, m . However, if one truncates perturbation series at a certain order they depend on it. One can determine this arbitrary parameter so that the correction terms are as small as possible. We adopt the following condition [1]:

$$\Pi_\pi(k^2 = m_{0\pi}^2) + \Pi_\pi(k = 0; T) = 0, \quad (\text{VI.65})$$

where the first and second terms are respectively T -independent part and T -dependent part of the one-loop self-energy of π .

Let us now turn to the discussion on the spectral function of σ defined by Eq.(II.24):

$$\rho_\sigma(k_0, \mathbf{k}) = -\frac{1}{\pi} \frac{\text{Im}\bar{\Pi}_\sigma(k_0, \mathbf{k})}{(k^2 - m_{0\sigma}^2 - \text{Re}\bar{\Pi}_\sigma(k_0, \mathbf{k}))^2 + (\text{Im}\bar{\Pi}_\sigma(k_0, \mathbf{k}))^2}. \quad (\text{VI.66})$$

Here $\bar{\Pi}_\sigma(k_0, \mathbf{k})$ is the self-energy of σ . Its real and imaginary parts are related with (1,1) component, Π_σ^{11} , *via* Eqs.(II.13) and (II.14).

As was already mentioned, the spectral function at one-loop order was studied by Chiku and Hatsuda [1]. We want to see how the spectral function at one-loop order is modified by adding the thermal sunset diagram. Thus, we take

$$\Pi_\sigma^{11}(k_0, \mathbf{k}) = \Pi_\sigma^{11}(k_0, \mathbf{k})_{1\text{-loop}} + \Pi_\sigma^{11}(k_0, \mathbf{k})_{\text{sunset}}. \quad (\text{VI.67})$$

The first term is the renormalized one-loop self-energy calculated in [1]. The second term is the renormalized sunset diagram depicted in Fig.5 and given by

$$\Pi_\sigma^{11}(k_0, \mathbf{k})_{\text{sunset}} = -\frac{\lambda^2}{6} i\mathcal{I}_{\text{sunset}}(k_0, \mathbf{k}; m_{0\pi}, m_{0\pi}, m_{0\sigma})_{11}. \quad (\text{VI.68})$$

We show $\rho_\sigma(k_0, \mathbf{k} = \mathbf{0})$ at $T = 200$ MeV and $T = 145$ MeV in Fig.6. At $T = 200$ MeV,

the spectral function at one-loop order consists of a δ -function peak for σ and a continuum. By including the sunset diagram σ acquires a width of the order of 10 MeV. At lower temperature, $T = 145$ MeV, an enhancement of the spectrum near the threshold is observed at one-loop order. When we include the sunset diagram, this feature is not lost.

Let us discuss the above results. At high temperature ($T = 200$ MeV), the mass of σ is smaller than twice the pion mass and the decay $\sigma \rightarrow \pi\pi$ is forbidden. As a result, within the one-loop calculation σ has zero width. However, at finite temperature σ can interact with thermal particles in heat bath and change into other states. Among such processes, those which are taken into account by including the sunset diagram are represented by Fig.3 with $(\Phi, \phi_1, \phi_2, \phi_3)$ assigned to, for example, $(\sigma, \sigma, \pi, \pi)$. The processes which correspond to (a) and (b) in Fig.3 are possible for $k_0 > 2m_{0\pi} + m_{0\sigma}$. This affect the spectrum at high energy. (c) and (d) in Fig.3 drop off for positive k_0 . (e) and (f) affect the spectrum at low energy since they are possible for $k_0 < m_{0\sigma} - 2m_{0\pi}$. The processes which correspond to (g) and (h) in Fig.3 are shown in Fig.7. They are the most important and give a finite width to σ since they are allowed at arbitrary positive k_0 . However, we observe that their effects at lower temperature ($T = 145$ MeV) are small. The reason is traced back to Eq.(IV.50). The term representing the probabilities for (g) and (h) in Fig.3 is the fourth term. That integral at lower temperature is suppressed due to the statistical weight since at lower temperature the masses of σ and π are large.

Finally we note that, as a consequence of the non-vanishing discontinuous part of the sunset diagram, the spectral function is also non-vanishing in the all range of k_0 .

VII. SUMMARY AND PERSPECTIVE

We have studied the sunset diagram for scalar field theories at finite temperature in the real time formalism. We have explained how we can reduce it to an expression written in terms of one-loop self-energy integrals, which can be easily evaluated numerically. We have also discussed what physical processes are contained in the discontinuous part of the diagram. We have found that there exist processes which occur only at finite temperature and some of them are allowed at arbitrary energy. As a result, the discontinuous part of the sunset diagram is non-vanishing in all the energy region, which is a remarkable feature at finite temperature and manifests itself at two-loop order.

As an application of the result, we have demonstrated how the spectral function of σ at finite T at one-loop order is modified when we include the thermal sunset diagram. At high temperature, where $\sigma \rightarrow \pi\pi$ is forbidden, σ acquires a finite width of the order of 10 MeV due to collisions with thermal particles in the heat bath while σ does not have a width at one-loop order. At lower temperature the spectrum is almost unchanged.

Finally we comment on the effect of other two-loop diagrams on the spectral function. We have seen that the threshold enhancement, which was first found in the one-loop calculation, is retained if we include the sunset diagram. However, in the present calculation the effect of the thermal width of π in the $\sigma \rightarrow \pi\pi$ decay is not included. This is taken into account by including the diagrams such as shown in Fig.8, in which an internal π changes into σ absorbing a thermal π in the heat bath.

In the one-loop calculation, π has a width, $\Gamma_\pi = 50$ MeV, at the temperature, $T = 145$ MeV, at which the threshold enhancement is observed for σ . If we include this effect as a constant complex mass shift for π in the one-loop self-energy for σ , we expect σ to acquire a width twice as that for π , i.e. $\Gamma_\sigma = 2\Gamma_\pi$ [25]. This implies that when the two-loop diagrams such as Fig.8 are included the spectral function for σ would be significantly modified with the width of about 100 MeV. The calculations of those diagrams are now in progress [26].

Acknowledgments

The authors would like to thank M. Ohtani for useful discussion. This work was partially supported by Grants-in-Aid of the Japanese Ministry of Education, Science, Sports, Culture and Technology (No.06572).

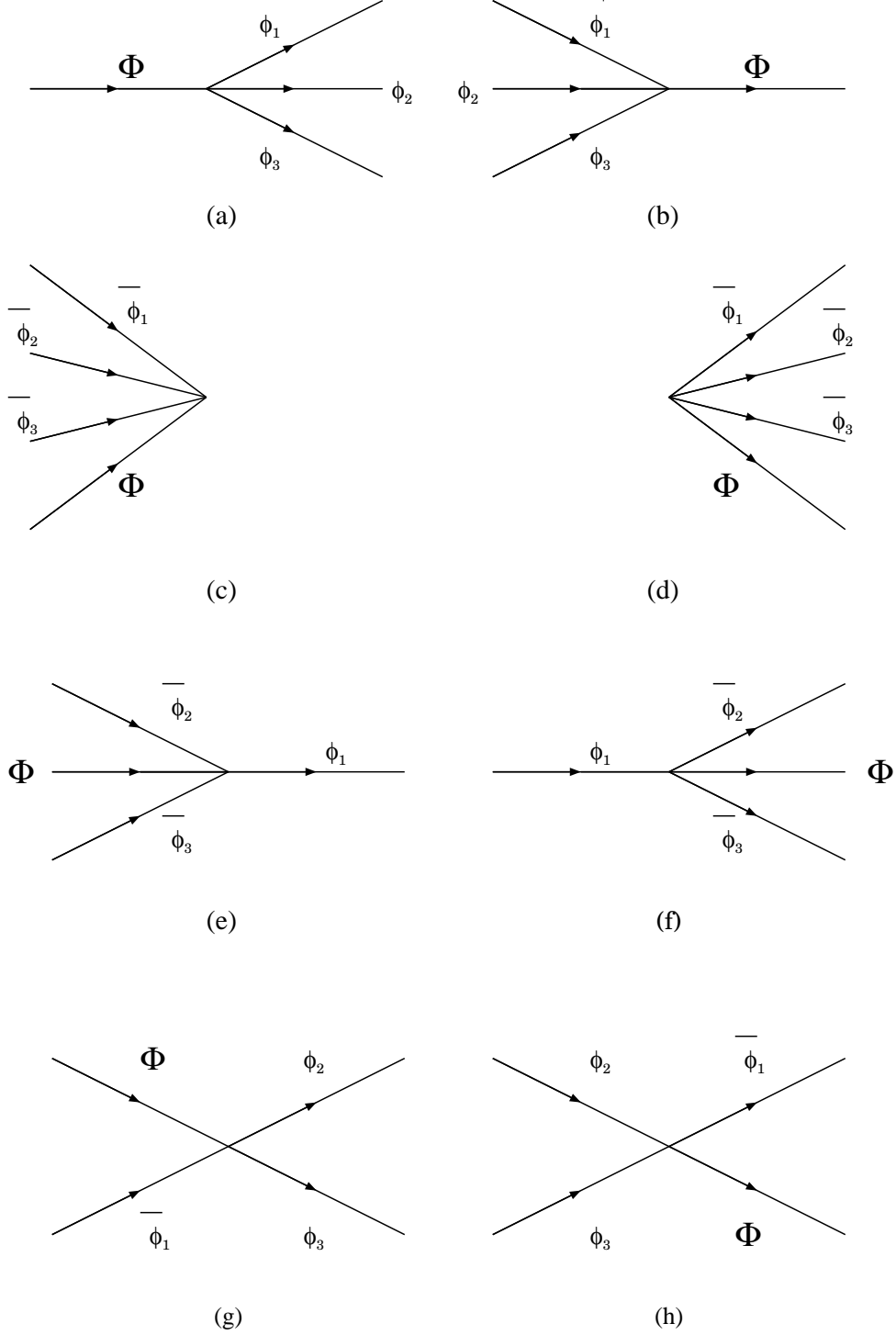


FIG. 3: The amplitudes in Eq.(IV.50) responsible for the disappearance and reappearance of Φ . $\bar{\phi}_i$ stands for an anti-particle of ϕ_i . (a) minus (b) corresponds to the first term in Eq.(IV.50), (c) minus (d) to the second, (e) minus (f) to the third and (g) minus (h) to the fourth. Amplitudes obtained by permuting particle labels of (e), (f), (g) and (h) also exist.

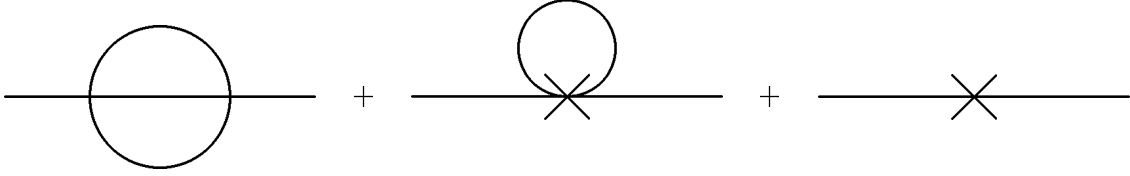


FIG. 4: Renormalized T -independent part of the sunset diagram. The second and the third diagrams cancel the sub- and overall divergences in the first diagram (bare sunset diagram) respectively.

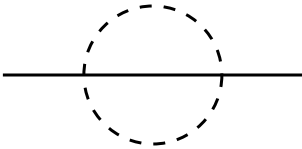


FIG. 5: The sunset diagram for σ . Solid and dashed lines correspond to σ and π respectively.

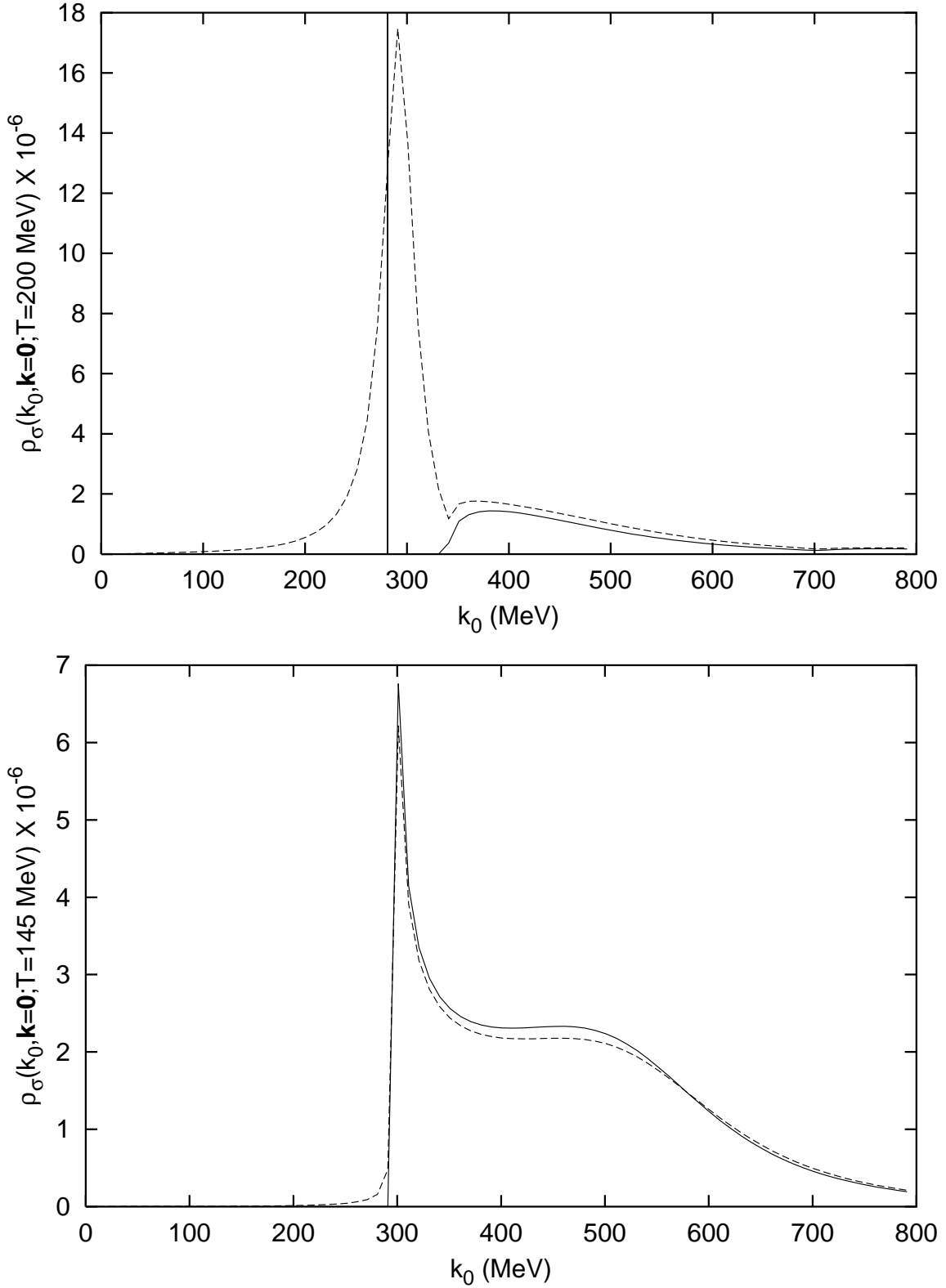


FIG. 6: Spectral function of σ $\rho_\sigma(k_0, \mathbf{k} = \mathbf{0})$ at $T = 200$ MeV (upper panel) and $T = 145$ MeV (lower panel). Solid line corresponds to ρ_σ at one-loop order and dashed line to that with one-loop self-energy and the sunset diagram.

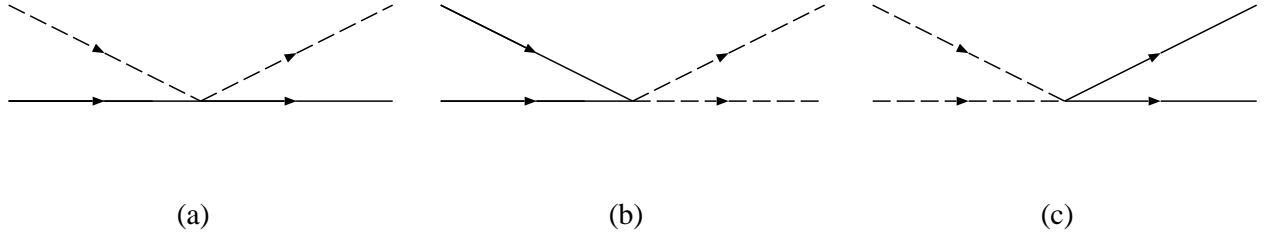


FIG. 7: The processes which are allowed at all positive k_0 contained in the discontinuous part of the sunset diagram for σ (Fig.5).

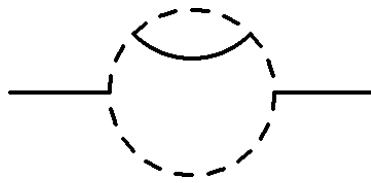


FIG. 8: two-loop self-energy diagram in which internal π changes into σ by absorbing thermal π in the heat bath.

APPENDIX A: CALCULATION OF $\text{Im}iF^{(2)}(p; m_1, m_2)$ AND $F^{(3)}(p; m_1, m_2)$

In this appendix, we derive Eqs.(III.35)-(III.37) and Eqs.(III.39)-(III.41).

From Eq.(III.28) we obtain

$$\begin{aligned} \text{Im}iF^{(2)}(p; m_1, m_2) &= \frac{1}{2} \int \frac{d^4k}{(2\pi)^4} 2\pi\delta((p+k)^2 - m_1^2)n(k_0)2\pi\delta(k^2 - m_2^2) \\ &= \frac{1}{4\pi} \int_{-\infty}^{\infty} dk_0 \int_0^{\infty} d|\mathbf{k}||\mathbf{k}|^2 n(k_0)\delta(k^2 - m_2^2) \\ &\quad \times \int_{-1}^1 d\cos\theta\delta(p^2 + 2p_0k_0 - 2|\mathbf{p}||\mathbf{k}|\cos\theta + k^2 - m_1^2). \end{aligned} \quad (\text{A.1})$$

$\text{Im}iF^{(2)}(p; m_1, m_2)$ receives contribution from k which satisfies

$$\frac{|p^2 + 2p_0k_0 + m_2^2 - m_1^2|}{2|\mathbf{p}||\mathbf{k}|} < 1 \quad (\text{A.2})$$

and $k_0^2 = \mathbf{k}^2 + m_2^2$. We make a square of Eq.(A.2) and obtain

$$4p_0k_0(p^2 + m_2^2 - m_1^2) < -(p^2 + m_2^2 - m_1^2)^2 - 4p_0^2m_2^2 - 4p^2|\mathbf{k}|^2. \quad (\text{A.3})$$

There are three cases when Eq.(A.3) holds:

- A. $\text{LHS} > 0$ and $\text{RHS} > 0$, $(\text{RHS})^2 - (\text{LHS})^2 > 0$.
- B. $\text{LHS} < 0$ and $\text{RHS} < 0$, $(\text{RHS})^2 - (\text{LHS})^2 < 0$.
- C. $\text{LHS} < 0$ and $\text{RHS} > 0$.

First, we calculate $(\text{RHS})^2 - (\text{LHS})^2$.

$$\begin{aligned} &(\text{RHS})^2 - (\text{LHS})^2 \\ &= 16p^4|\mathbf{k}|^4 + \{8p^2[(p^2 + m_2^2 - m_1^2)^2 + 4p_0^2m_2^2] - 16(p^2 + m_2^2 - m_1^2)^2p_0^2\}|\mathbf{k}|^2 \\ &\quad + [(p^2 + m_2^2 - m_1^2)^2 + 4p_0^2m_2^2]^2 - 16(p^2 + m_2^2 - m_1^2)^2p_0^2m_2^2 \\ &= 16p^4|\mathbf{k}|^4 + 8[(p^2 - 2p_0^2)(p^2 + m_2^2 - m_1^2)^2 + 4p^2p_0^2m_2^2]|\mathbf{k}|^2 \\ &\quad + [(p^2 + m_2^2 - m_1^2)^2 - 4p_0^2m_2^2]^2 \end{aligned} \quad (\text{A.4})$$

Whether there exists $|\mathbf{k}|^2$ which satisfies $(\text{RHS})^2 - (\text{LHS})^2 < 0$ depends on the sign of the following expression:

$$\begin{aligned} D &= 16[(p^2 - 2p_0^2)(p^2 + m_2^2 - m_1^2)^2 + 4p^2p_0^2m_2^2]^2 - 16p^4[(p^2 + m_2^2 - m_1^2)^2 - 4p_0^2m_2^2]^2 \\ &= 64p_0^2|\mathbf{p}|^2(p^2 + m_2^2 - m_1^2)^2[p^2 - (m_1 + m_2)^2][p^2 - (m_1 - m_2)^2]. \end{aligned} \quad (\text{A.5})$$

Thus, for $(m_1 - m_2)^2 < p^2 < (m_1 + m_2)^2$

$$(\text{RHS})^2 - (\text{LHS})^2 > 0,$$

for $p^2 < (m_1 - m_2)^2$ or $(m_1 + m_2)^2 < p^2$

$$\begin{aligned} |\mathbf{k}|^2 < |\mathbf{k}|_-^2 \quad \text{or} \quad |\mathbf{k}|^2 > |\mathbf{k}|_+^2 &\iff (\text{RHS})^2 - (\text{LHS})^2 > 0, \\ |\mathbf{k}|_-^2 < |\mathbf{k}|^2 < |\mathbf{k}|_+^2 &\iff (\text{RHS})^2 - (\text{LHS})^2 < 0, \end{aligned}$$

where $|\mathbf{k}|_\pm^2$ are given by

$$|\mathbf{k}|_\pm^2 = \frac{1}{4} \left\{ \sqrt{\left(1 + \frac{m_2^2 - m_1^2}{p^2}\right)^2} |\mathbf{p}| \pm \sqrt{\left[1 - \frac{(m_2 + m_1)^2}{p^2}\right] \left[1 - \frac{(m_1 - m_2)^2}{p^2}\right]} |p_0| \right\}^2. \quad (\text{A.6})$$

Secondly, for $p^2 > m_1^2 - m_2^2$

$$p_0 k_0 \geq 0 \iff \text{LHS} \geq 0,$$

for $p^2 < m_1^2 - m_2^2$

$$p_0 k_0 \geq 0 \iff \text{LHS} \leq 0.$$

Thirdly, for $p^2 > 0$

$$\text{RHS} < 0$$

for $p^2 < 0$

$$|\mathbf{k}|^2 \geq \frac{(p^2 + m_2^2 - m_1^2)^2 + 4p_0^2 m_2^2}{-4p^2} \equiv |\mathbf{k}|_0^2 \iff \text{RHS} \geq 0$$

Therefore, the conditions for the above three cases are respectively given by

A. $p^2 < 0$, $p_0 k_0 (p^2 + m_2^2 - m_1^2) > 0$ and $|\mathbf{k}|^2 > |\mathbf{k}|_+^2$.

B. $p^2 > (m_1 + m_2)^2$, $p_0 k_0 (p^2 + m_2^2 - m_1^2) < 0$ and $|\mathbf{k}|_-^2 < |\mathbf{k}|^2 < |\mathbf{k}|_+^2$,

$0 < p^2 < (m_1 - m_2)^2$ and $p_0 k_0 (p^2 + m_2^2 - m_1^2) < 0$ and $|\mathbf{k}|_-^2 < |\mathbf{k}|^2 < |\mathbf{k}|_+^2$,

$p^2 < 0$, $p_0 k_0 (p^2 + m_2^2 - m_1^2) < 0$ and $|\mathbf{k}|_-^2 < |\mathbf{k}|^2 < |\mathbf{k}|_0^2$.

C. $p^2 < 0$, $p_0 k_0 (p^2 + m_2^2 - m_1^2) < 0$ and $|\mathbf{k}|^2 > |\mathbf{k}|_0^2$.

The case C can be combined with the third of the case B as

$p^2 < 0$, $p_0 k_0(p^2 + m_2^2 - m_1^2) < 0$ and $|\mathbf{k}|^2 > |\mathbf{k}|_-^2$.

1. For $p^2 > (m_1 + m_2)^2$ or $0 < p^2 < (m_1 - m_2)^2$,

$$\begin{aligned} \text{Im}iF^{(2)}(p; m_1, m_2) &= \frac{1}{8\pi|\mathbf{p}|} \int_{|\mathbf{k}|_-}^{|\mathbf{k}|_+} d|\mathbf{k}| \frac{|\mathbf{k}|}{\omega_k} n(\omega_k) \\ &= \frac{1}{8\pi|\mathbf{p}|} \int_{\omega_-}^{\omega_+} d\omega n(\omega) \\ &= \frac{1}{16\pi|\mathbf{p}|} \frac{1}{\beta} \ln \left| \frac{1 - e^{-\beta\omega_+}}{1 - e^{-\beta\omega_-}} \right|. \end{aligned} \quad (\text{A.7})$$

2. For $(m_1 - m_2)^2 < p^2 < (m_1 + m_2)^2$,

$$\text{Im}iF^{(2)}(p; m_1, m_2) = 0. \quad (\text{A.8})$$

3. For $p^2 < 0$,

$$\begin{aligned} \text{Im}iF^{(2)}(p; m_1, m_2) &= \frac{1}{8\pi|\mathbf{p}|} \left(\int_{|\mathbf{k}|_-}^{\infty} + \int_{|\mathbf{k}|_+}^{\infty} \right) d|\mathbf{k}| \frac{|\mathbf{k}|}{\omega_k} n(\omega_k) \\ &= \frac{1}{8\pi|\mathbf{p}|} \left(\int_{\omega_-}^{\infty} + \int_{\omega_+}^{\infty} \right) d\omega n(\omega) \\ &= \frac{1}{16\pi|\mathbf{p}|} \frac{-1}{\beta} \ln |(1 - e^{-\beta\omega_+})(1 - e^{-\beta\omega_-})|. \end{aligned} \quad (\text{A.9})$$

where

$$\omega_{\pm} = \frac{1}{2} \left| \sqrt{\left(1 + \frac{m_2^2 - m_1^2}{p^2}\right)^2} |p_0| \pm \sqrt{\left[1 - \frac{(m_2 + m_1)^2}{p^2}\right] \left[1 - \frac{(m_1 - m_2)^2}{p^2}\right]} |\mathbf{p}| \right| \quad (\text{A.10})$$

Similarly,

1. For $p^2 > (m_1 + m_2)^2$,

$$\begin{aligned} \text{Im}iF^{(3)}(p; m_1, m_2) &= \frac{1}{8\pi|\mathbf{p}|} \int_{|\mathbf{k}|_-}^{|\mathbf{k}|_+} d|\mathbf{k}| \frac{|\mathbf{k}|}{\omega_k} n(\omega_k) n(|p_0| - \omega_k) \\ &= \frac{1}{8\pi|\mathbf{p}|} \int_{\omega_-}^{\omega_+} d\omega n(\omega) n(|p_0| - \omega) \\ &= \frac{1}{8\pi|\mathbf{p}|} \frac{1}{\beta} \frac{1}{e^{\beta|p_0|} - 1} \ln \left| \frac{1 - e^{-\beta\omega_+} e^{\beta(|p_0| - \omega_-)} - 1}{1 - e^{-\beta\omega_-} e^{\beta(|p_0| - \omega_+)} - 1} \right|. \end{aligned} \quad (\text{A.11})$$

2. For $(m_1 - m_2)^2 < p^2 < (m_1 + m_2)^2$,

$$\text{Im}iF^{(3)}(p; m_1, m_2) = 0. \quad (\text{A.12})$$

3. For $0 < p^2 < (m_1 - m_2)^2$,

$$\begin{aligned}
\text{Im}iF^{(3)}(p; m_1, m_2) &= \frac{1}{8\pi|\mathbf{p}|} \int_{|\mathbf{k}|_-}^{|\mathbf{k}|_+} d|\mathbf{k}| \frac{|\mathbf{k}|}{\omega_k} n(\omega_k) n(|p_0| + \omega_k) \\
&= \frac{1}{8\pi|\mathbf{p}|} \int_{\omega_-}^{\omega_+} d\omega n(\omega) n(|p_0| + \omega) \\
&= \frac{1}{8\pi|\mathbf{p}|\beta} \cdot \frac{1}{e^{\beta|p_0|} - 1} \\
&\quad \times \left[\ln \left| \frac{1 - e^{-\beta\omega_+}}{1 - e^{-\beta\omega_-}} \right| - e^{\beta|p_0|} \ln \left| \frac{1 - e^{-\beta(|p_0| + \omega_+)}}{1 - e^{-\beta(|p_0| + \omega_-)}} \right| \right]. \quad (\text{A.13})
\end{aligned}$$

4. For $p^2 < 0$,

$$\begin{aligned}
&\text{Im}iF^{(3)}(p; m_1, m_2) \\
&= \frac{1}{8\pi|\mathbf{p}|} \left(\int_{|\mathbf{k}|_-}^{\infty} d|\mathbf{k}| \frac{|\mathbf{k}|}{\omega_k} n(\omega_k) n(|p_0| + \omega_k) + \int_{|\mathbf{k}|_+}^{\infty} d|\mathbf{k}| \frac{|\mathbf{k}|}{\omega_k} n(\omega_k) n(|p_0| - \omega_k) \right) \\
&= \frac{1}{8\pi|\mathbf{p}|} \left(\int_{\omega_-}^{\infty} d\omega n(\omega) n(|p_0| + \omega) + \int_{\omega_+}^{\infty} d\omega n(\omega) n(|p_0| - \omega) \right) \\
&= \frac{1}{8\pi|\mathbf{p}|\beta} \left\{ \frac{1}{e^{-\beta|p_0|} - 1} [-\ln|1 - e^{-\beta\omega_+}| + e^{-\beta|p_0|} \ln|1 - e^{-\beta(\omega_+ - |p_0|)}|] \right. \\
&\quad \left. + \frac{1}{e^{\beta|p_0|} - 1} [-\ln|1 - e^{-\beta\omega_-}| + e^{\beta|p_0|} \ln|1 - e^{-\beta(\omega_- + |p_0|)}|] \right\}. \quad (\text{A.14})
\end{aligned}$$

APPENDIX B: PHYSICAL MEANING OF $|\mathbf{k}|_{\pm}$

In this appendix we explain the physical meaning of $|\mathbf{k}|_{\pm}$ defined by Eq.(A.6).

Let us first consider the case $p^2 > (m_1 + m_2)^2$ or $0 < p^2 < (m_1 - m_2)^2$. For simplicity we suppose $p_0 > 0$. Since internal particles are on shell, in the center-of-mass frame we have

$$p^2 = \left(\sqrt{m_1^2 + |\mathbf{k}|^2} \pm \sqrt{m_2^2 + |\mathbf{k}|^2} \right)^2, \quad (\text{B.1})$$

where $+$ is for $p^2 > (m_1 + m_2)^2$ and $-$ is for $0 < p^2 < (m_1 - m_2)^2$. In either case

$$|\mathbf{k}|^2 = \frac{[p^2 - (m_1 + m_2)^2][p^2 - (m_1 - m_2)^2]}{4p^2}. \quad (\text{B.2})$$

If we boost the system to the positive z-direction, the external and internal momenta become

$$\begin{cases} p'_0 = p_0 \cosh\theta, \\ \mathbf{p}'_{\perp} = 0, \quad p'_z = p_0 \sinh\theta \quad (\theta > 0), \end{cases} \quad (\text{B.3})$$

$$\begin{cases} k'_0 = k_0 \cosh\theta + k_z \sinh\theta, \\ \mathbf{k}'_{\perp} = \mathbf{k}_{\perp}, \quad k'_z = k_z \cosh\theta + k_0 \sinh\theta. \end{cases} \quad (\text{B.4})$$

Since $-|\mathbf{k}| < k_z < |\mathbf{k}|$,

$$|\mathbf{k}'|_-^2 \leq |\mathbf{k}'|^2 \leq |\mathbf{k}'|_+^2, \quad (\text{B.5})$$

where

$$\begin{aligned} |\mathbf{k}'|_{\pm}^2 &= (\pm|\mathbf{k}|\cosh\theta + |k_0|\sinh\theta)^2 \\ &= \left(\pm|\mathbf{k}|\frac{p'_0}{p_0} + |k_0|\frac{p'_z}{p_0} \right)^2 \\ &= \frac{1}{4} \left\{ \pm\sqrt{\left[1 - \frac{(m_1 + m_2)^2}{p^2}\right] \left[1 - \frac{(m_1 - m_2)^2}{p^2}\right]} p'_0 + \left|1 + \frac{m_2^2 - m_1^2}{p^2}\right| |\mathbf{p}'| \right\}^2. \end{aligned} \quad (\text{B.6})$$

This is nothing but Eq.(A.6). Therefore, for $p^2 > (m_1 + m_2)^2$ or $0 < p^2 < (m_1 - m_2)^2$, $|\mathbf{k}|_+$ and $|\mathbf{k}|_-$ are respectively the maximum and minimum values of $|\mathbf{k}|$ such that the internal particles are on-shell.

Let us next consider the case $p^2 < 0$. In the Breit frame, $p = (0, \mathbf{p})$, with \mathbf{p} in the positive z-direction we write the momentum of the particle with mass m_2 by $k = (k_0, \mathbf{k})$ where k_0 can be positive or negative. Then, the momentum of the particle with mass $p + k = (k_0, \mathbf{p} + \mathbf{k})$. Since internal particles are on shell, we have

$$k_0^2 = m_2^2 + k_z^2 + |\mathbf{k}_{\perp}|^2 = m_1^2 + (p_z + k_z)^2 + |\mathbf{k}_{\perp}|^2. \quad (\text{B.7})$$

From this equation we obtain

$$\begin{aligned} k_z &= -\frac{p_z^2 + m_1^2 - m_2^2}{2p_z} = \frac{-p^2 + m_1^2 - m_2^2}{2\sqrt{-p^2}}, \\ k_0^2 &= \frac{[-p^2 + (m_1 + m_2)^2][-p^2 + (m_1 - m_2)^2]^2}{-4p^2} + |\mathbf{k}_{\perp}|^2, \end{aligned} \quad (\text{B.8})$$

When boosting the frame to the z-direction, we suppose the momenta become

$$p' = (p'_0, \mathbf{p}'), \quad k' = (k'_0, \mathbf{k}'), \quad p' + k' = (p'_0 + k'_0, \mathbf{p}' + \mathbf{k}'). \quad (\text{B.9})$$

Then, p' and k' are given by

$$\begin{cases} p'_0 = |\mathbf{p}'|\sinh\theta, \\ |\mathbf{p}'| = |\mathbf{p}|\cosh\theta, \end{cases} \quad (\text{B.10})$$

$$\begin{cases} k'_0 = k_0\cosh\theta + k_z\sinh\theta, \\ \mathbf{k}'_{\perp} = \mathbf{k}_{\perp}, \quad k'_z = k_z\cosh\theta + k_0\sinh\theta. \end{cases} \quad (\text{B.11})$$

Using Eqs.(B.8), (B.10) and (B.11), we obtain

$$|\mathbf{k}'|^2 = (k_z \cosh\theta + k_0 \sinh\theta)^2 + |\mathbf{k}_\perp|^2. \quad (\text{B.12})$$

$|\mathbf{k}'|^2$ has a minimum when $|\mathbf{k}_\perp|^2 = 0$ but not a maximum. Depending on the sign of k_0 , the minimum value is given by

$$\begin{aligned} |\mathbf{k}'|_\pm^2 &= \left(|k_z| \frac{|\mathbf{p}'|}{\sqrt{-p^2}} \pm \sqrt{k_z^2 + m_2^2} \frac{p'_0}{\sqrt{-p^2}} \right)^2 \\ &= \frac{1}{4} \left\{ \left| 1 - \frac{m_1^2 - m_2^2}{-p^2} \right| |\mathbf{p}'| \pm \sqrt{\left[1 + \frac{(m_1 + m_2)^2}{-p^2} \right] \left[1 + \frac{(m_1 - m_2)^2}{-p^2} \right]} p'_0 \right\}^2. \end{aligned} \quad (\text{B.13})$$

Eq.(B.13) is nothing but Eq.(A.6). Therefore, in the case of $p^2 < 0$, both of $|\mathbf{k}|_+$ and $|\mathbf{k}|_-$ are the minimum values of $|\mathbf{k}|$ such that the internal particles can be on-shell.

References

- [1] S. Chiku and T. Hatsuda, Phys. Rev. **D57**, R6 (1998); Phys. Rev. **D58**, 76001 (1998)
- [2] J. Schwinger, J. Math. Phys. **2**, 407 (1961).
- [3] L.V. Keldysh, JETP(Sov. Phys.) **20**, 1018 (1964).
- [4] R.A. Craig, J. Math. Phys. **9**, 605 (1968).
- [5] G.-Z. Zhou, Z.-B. Su, B.-L Hao and Lu Yu, Phys. Rev. **B22**, 3385 (1980).
- [6] Y. Takahashi and H. Umezawa, Coll. Phen. **2**, 55 (1975).
- [7] G.W. Semenoff and Y. Takahashi, Nucl. Phys. **B220**[FS8], 196 (1983).
- [8] I.P. Kadanoff and G. Baym, Quantum Statistical Mechanics (Benjamin, New York 1969); D.C. Langreth, in 1975 NATO ADI on Linear and Non-Linear Electron Transport in Solids, J.T. Devreese and E. van Boem eds. (Plenum, New York 1976)
- [9] R. Mills, Propagators for many-particle systems (Gordon and Breach, New York 1969)
- [10] E.M. Lifshitz and L.P. Pitaevskii, Course of theoretical physics, vol.10: Physical kinetics (Pergamon, New York 1981).
- [11] H. Umezawa, H. Matsumoto and M. Tachiki, Thermofield Dynamics and Condensed States (North-Holland, Amsterdam, 1982).
- [12] A.J. Niemi and G.W. Semenoff, Ann. Phys. **152**, 105 (1984).
- [13] A.J. Niemi and G.W. Semenoff, Nucl. Phys. **B230**, 181 (1984).
- [14] M. Lebellac, *Thermal Field Theory*, Cambridge University Press 1996.
- [15] G.W. Semenoff and H. Umezawa, Nucl. Phys. **B220**, 196 (1983)
- [16] See, for example, P. Ramond, *Field Theory, A Modern Primer* (Benjamin/Cummings, New York, 1981).
- [17] Y. Fujimoto, M. Morikawa and M. Sasaki, Phys. Rev. **D33**, 590 (1986).
- [18] H.A. Weldon, Phys. Rev. **D28**, 2007 (1983).
- [19] P. Post and J.B. Tausk, Mod. Phys. Lett. **A11**, 2115 (1996).
- [20] J. Gasser and M.E. Sainio, Eur. Phys. J. **C6**, 297 (1999).

- [21] J.O. Andersen and E. Braaten, Phys. Rev. **D62**, 45004 (2000); Phys. Rev. **D51**, 6990 (1995).
- [22] S. Groote, J.G. Koelner and A.A. Pivovarov, Phys. Lett. **B443**, 269 (1998); Nucl. Phys. **B542**, 515 (1999); Eur. Phys. J. **C11**, 279 (1999).
- [23] S. Weinberg, Phys. Rev. **D9**, 3357 (1974);
L. Dolan and R. Jackiw, Phys. Rev. **D9**, 3320 (1974).
- [24] D.A. Kirzhnits and A.D. Linde, Ann. Phys. (N.Y.) **101**, 195 (1976).
- [25] T. Nishikawa, O. Morimatsu, Y. Hidaka and M. Ohtani, in preparation.
- [26] T. Nishikawa, O. Morimatsu and Y. Hidaka, in preparation.